Journal of Sound and Vibration (2002) **255**(2), 337–355
doi:10.1006/jsvi.2001.4158, available online at http://www.idealibrary.com on IDEAL®

TRACKING CONTROL OF THE FLEXIBLE SLIDER–CRANK MECHANISM SYSTEM UNDER IMPACT

R.-F. FUNG AND J.-H. SUN

Department of Mechanical and Automation Engineering, National Kaohsiung First University of Science and Technology, University Road, Yenchau, Kaohsiung, Taiwan 824, *Republic of China.*
E-mail: rffung@ccms.nkfust.edu.tw

AND

J.-W. WU

Department of Mechanical Engineering, Chung Yuan Christian University, Chung-Li, Taiwan 32023, *Republic of China*

(*Received* 1 *March* 2001, *and in final form* 9 *November* 2001)

The variable structure control (VSC) and the stabilizer design by using pole placement technique are applied to the tracking control of the flexible slider–crank mechanism under impact. The VSC strategy is employed to track the crank angular position and speed, while the stabilizer design is involved to suppress the flexible vibrations simultaneously. From the theoretical impact consideration, three approaches including the generalized momentum balance (GMB), the continuous force model (CFM), and the CFM associated with the effective mass compensation EMC are adopted, and are derived on the basis of the energy and impulse–momentum conservations. Simulation results are provided to demonstrate the performance of the motor-controller flexible slider–crank mechanism not only accomplishing good tracking trajectory of the crank angle, but also eliminating vibrations of the flexible connecting rod.

1. INTRODUCTION

Multibody dynamics is an important tool in the design and simulation of complex mechanism systems. The dynamic analysis of a slider–crank mechanism has been studied extensively over the past 40 years with much of the research going beyond the current paper to include totally flexible mechanisms. An excellent survey of these works related to the topic of flexible mechanisms is given by Erdman [1]. The slider–crank mechanism has been conventionally designed on the basis of the assumption that all members in the mechanism are rigid bodies. There will be some problems in the mechanism when the vibrations are greater than the allowable limit.

In order to obtain a more accurate prediction of the motion of the slider–crank mechanism, dynamics analysis of its flexible connecting rod is necessary. Lieh [2] investigated dynamic behavior of the slider–crank mechanism with the flexible coupler and joint, in which the equations were linearized under the assumption of small deformation. Fallahi *et al.* [3] also developed a finite element formulation to analyze the flexible slider–crank mechanism system in which a local co-ordinate system was employed. Fung [4] dynamically analyzed the slider–crank mechanism with the flexible connecting rod, which was modelled by Timoshenko-beam theory. Hsiao and Yang [5] presented

0022-460X/02/$35.00

a co-rotational finite element formulation of a slender curve beam element. A finite element method for dynamic analysis of a flexible connecting rod of the slider–crank mechanism with a time-dependent boundary condition was presented by Fung and Chen [6]. In the previous studies, the motor was not used to drive the mechanism and no control law was designed to control the mechanism. Recently, Fung and Chen [7] have focused on the vibration control of the slider–crank mechanism system driven by a permanent magnet (PM) synchronous servo motor.

The dynamic analyses of impact are cataloged as the generalized momentum balance (GME), the continuous force model (CFM), and the CFM associated with the effective mass compensation (EMC). Two important researches of impact can be found as follows. Khulief and Shabana [8] introduced the GMB approach to evaluate the impact problem for the multibody systems, and also derived the so-called CFM approach [9] for the multibody systems under impact. Additionally, a new concept called the CFM associated with the EMC [9] was developed for the impact occurring not only on two colliding bodies but also on two subsystems. However, the motor was not used to drive the mechanism and no control law was designed to control the rigid-body motion and flexible vibration in the previous studies [8, 9].

The most distinguishing feature of the VSC is its ability to demonstrate the performance of robustness with respect to parameter variations and external disturbances [10, 11]. Most of the developments of the VSC approach are focused on the rigid-body motion of a robot arm. However, Yeung and Chen [12–14] presented an approximate closed-form approach by linearizing the non-linear dynamic equation of a flexible robot arm. The pole placement technique [12] and the PD/PID compensations [13, 14] were utilized to stabilize the linearized time-invariant system. Nathan and Singh [15], Ficola *et al.* [16], and Choi *et al.* [17] investigated the flexible robotic arm via the VSC controller for joint angles. The pole assignment technique [15] was employed to design a stabilizer, which damps the elastic oscillation of the linearized model.

To the authors' knowledge, there are few papers concerning the motor-controller flexible slider–crank mechanism under impact. The main aim of this paper is to track the angular position and speed of the flexible slider–crank mechanism driven by a controlled PM synchronous servo motor. Meanwhile, three dynamic analyses of impact, i.e., the GMB, the CFM, and the CFM associated with the EMC, are developed for the motor-controller flexible slider–crank mechanism system. The VSC algorithm is designed to track the angular crank position and speed, while the stabilizer design [15] is employed to suppress the flexible vibration problem. Finally, simulation results are provided to validate the theoretical analysis.

2. DYNAMIC ANALYSIS

Figure 1 shows the physical model of a slider–crank mechanism associated with a flexible connecting rod driven by a PM synchronous servo motor [7]. In the kinematic analysis, constraint equations often occur in the mechanism. The co-ordinate partitioning method [18] partitions the co-ordinate vector as

$$\mathbf{Q} = [\mathbf{Q}_1 \;\; \mathbf{Q}_2 \cdots \mathbf{Q}_n]^{\mathrm{T}} = [\mathbf{p}^{\mathrm{T}} \;\; \mathbf{q}^{\mathrm{T}}]^{\mathrm{T}}, \tag{1}$$

where $\mathbf{p} = [p_1 \;\; p_2 \cdots p_m]^{\mathrm{T}}$ and $\mathbf{q} = [q_1 \;\; q_2 \cdots q_k]^{\mathrm{T}}$ are the m-dependent and k-independent co-ordinates respectively. The m constraint equations may be expressed as

$$\mathbf{\Phi} \equiv \mathbf{\Phi}(\mathbf{Q}) \equiv \mathbf{\Phi}(\mathbf{p}, \mathbf{q}) = \mathbf{0}. \tag{2}$$

Constraint equations represented by equation (2) are usually non-linear.

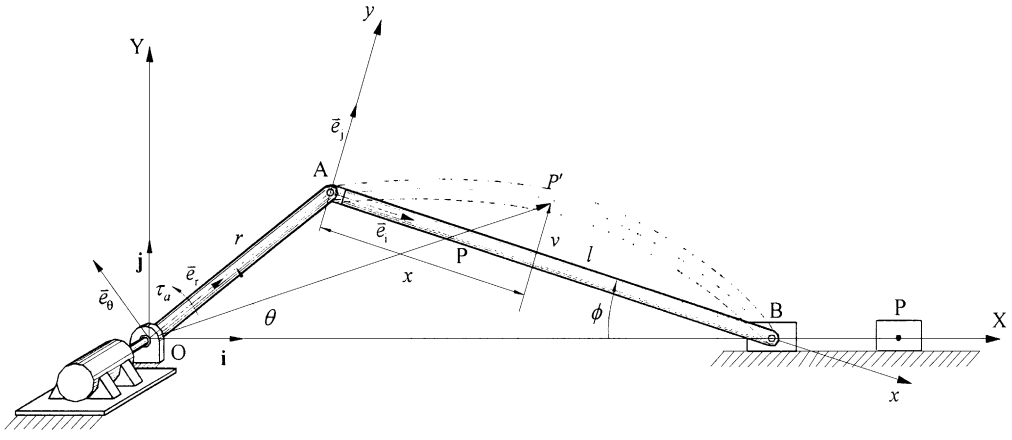

Figure 1. The motor-controller flexible slider–crank mechanism under impact.

In general situation, the Euler–Lagrange equation [19] accounting for both the applied and constraint forces, and the acceleration constraint equation can be combined into the matrix form as

$$\begin{bmatrix} \mathbf{M} & \Phi_Q^{\mathrm{T}} \\ \Phi_Q & \mathbf{0} \end{bmatrix} \begin{bmatrix} \ddot{\mathbf{Q}} \\ \lambda \end{bmatrix} = \begin{bmatrix} \mathbf{BU} - \mathbf{N}(\mathbf{Q}, \dot{\mathbf{Q}}) \\ \gamma \end{bmatrix}, \tag{3}$$

where $\mathbf{M}$ is the mass matrix, $\mathbf{N}$ is the non-linear vector, λ is the Lagrange multipliers, $\mathbf{B}$ is the constant matrix, $\mathbf{U}$ is the vector of control input, and $\gamma \equiv -(\Phi_Q \dot{\mathbf{Q}})_Q \dot{\mathbf{Q}}$. Equation (3) is a system of differential-algebraic equation (DAE).

Implicit function method will be employed to solve the DAE (3) by reordering and partitioning. According to the decomposition of $\mathbf{Q}$ into $\mathbf{p}$ and $\mathbf{q}$, we have

$$\begin{aligned} \mathbf{M}^{pp}\ddot{\mathbf{p}} + \mathbf{M}^{pq}\ddot{\mathbf{q}} + \Phi_p^{\mathrm{T}}\lambda &= \mathbf{B}^p\mathbf{U} - \mathbf{N}^p, \\ \mathbf{M}^{qp}\ddot{\mathbf{p}} + \mathbf{M}^{qq}\ddot{\mathbf{q}} + \Phi_q^{\mathrm{T}}\lambda &= \mathbf{B}^q\mathbf{U} - \mathbf{N}^q, \\ \Phi_p\ddot{\mathbf{p}} + \Phi_q\ddot{\mathbf{q}} &= \gamma. \end{aligned} \tag{4}$$

Eliminating λ and $\ddot{\mathbf{p}}$ yields

$$\hat{\mathbf{M}}(\mathbf{q})\ddot{\mathbf{q}} + \hat{\mathbf{N}}(\mathbf{q}, \dot{\mathbf{q}}) = \hat{\mathbf{Q}}\mathbf{U}, \tag{5}$$

where $\hat{\mathbf{M}}$, $\hat{\mathbf{N}}$, and $\hat{\mathbf{Q}}$ can be seen in reference [7]. Equation (5) is a set of differential equations in terms of the independent co-ordinate vector $\mathbf{q}$ only and is an initial-value problem. It should be noted that the independent co-ordinate vector $\mathbf{q}$ includes both the crank angle and the generalized co-ordinates of the flexible vibrations.

Let $\mathbf{X} = [\mathbf{q}, \dot{\mathbf{q}}]^{\mathrm{T}}$ be the state vector, one can rewrite equation (5) in terms of $\mathbf{X}$ as

$$\dot{\mathbf{X}} = \hat{\mathbf{a}}(\mathbf{X}) + \hat{\mathbf{b}}\mathbf{U}, \tag{6}$$

where

$$\hat{\mathbf{a}}(\mathbf{X}) = \begin{bmatrix} \dot{\mathbf{q}} \\ -\hat{\mathbf{M}}^{-1}\hat{\mathbf{N}} \end{bmatrix}, \qquad \hat{\mathbf{b}} = \begin{bmatrix} \mathbf{0} \\ \hat{\mathbf{M}}^{-1}\hat{\mathbf{Q}} \end{bmatrix}.$$

3. IMPACT ANALYSES OF THE MECHANISM SYSTEM

In this section, we consider the motion in a given stroke of the slider–crank mechanism undergoing impact when two bodies collide over a very short period of time. The three approaches [8, 9] in treating the impact problem are derived on the basis of the energy and impulse–momentum conservations and will be discussed as follows.

3.1. THE GMB APPROACH

Now, we consider the impact effect between two colliding bodies due to the impulsive force acting over a very short period of time in the slider–crank mechanism. The impact analysis of the GMB approach has the following assumptions:

(1) The system position is not changed and also the friction effect of impacting surfaces between two colliding bodies is not considered during the short time interval.
(2) By using the integral mean value theorem, it is assumed that **BU** in equation (3) is continuous and the velocities are bounded during impact. Thus, the integrals of **BU** and **N** are zero during the short time interval, $\Delta\tau = |\tau_i^+ - \tau_i^-| \to 0$.

Integrating the DAE (3) and considering the restitution between two impacting bodies, one has the matrix form [8, 20]

$$\begin{bmatrix} \mathbf{M} & \mathbf{\Phi}_Q^{\mathrm{T}} & \left\{\dfrac{\partial R_{ij}}{\partial \mathbf{Q}}\right\}^{\mathrm{T}} \\ \mathbf{\Phi}_Q & \mathbf{0} & \mathbf{0} \\ \left\{\dfrac{\partial R_{ij}}{\partial \mathbf{Q}}\right\} & \mathbf{0} & \mathbf{0} \end{bmatrix} \begin{bmatrix} \Delta\dot{\mathbf{Q}} \\ \mathbf{H}^{\lambda} \\ -\mathbf{H} \end{bmatrix} = \begin{bmatrix} \mathbf{0} \\ \mathbf{0} \\ -(1+r_e)\left\{\dfrac{\partial R_{ij}}{\partial \mathbf{Q}}\right\}\dot{\mathbf{Q}}(t_i^-) \end{bmatrix}, \tag{7}$$

where R_{ij} is the relative displacement or penetration in the common normal direction for bodies i and j, $\mathbf{\Phi}_Q^{\mathrm{T}}\mathbf{H}^{\lambda}$ is the generalized impulse of the constraint reaction force with $\mathbf{H}^{\lambda} = \lim_{\Delta t \to 0} \int_{\tau_i^-}^{\tau_i^+} \lambda \, \mathrm{d}t$ and $\mathbf{P} = \{\partial R_{ij}/\partial \mathbf{Q}\}^{\mathrm{T}}\mathbf{H}$, in which the generalized impulse $\mathbf{H} = \lim_{\Delta\tau \to 0} \int_{\tau_i^-}^{\tau_i^+} F(t)\,\mathrm{d}t$, r_e is the coefficient of restitution for describing the impact characteristics between two bodies, and $\Delta\dot{\mathbf{Q}}$ is the jump discontinuity of velocity in the instantaneous time of impacting.

According to the decomposition of $\mathbf{Q}$ into $\mathbf{p}$ and $\mathbf{q}$, equation (7) becomes

$$\begin{aligned} &\mathbf{M}^{pp}\Delta\dot{\mathbf{p}} + \mathbf{M}^{pq}\Delta\dot{\mathbf{q}} + \Phi_p^{\mathrm{T}}\mathbf{H}^{\lambda} - (R_{ij})_p^{\mathrm{T}}\mathbf{H} = \mathbf{0}, \\ &\mathbf{M}^{qp}\Delta\dot{\mathbf{p}} + \mathbf{M}^{qq}\Delta\dot{\mathbf{q}} + \Phi_q^{\mathrm{T}}\mathbf{H}^{\lambda} - (R_{ij})_q^{\mathrm{T}}\mathbf{H} = \mathbf{0}, \\ &\mathbf{\Phi}_p\Delta\dot{\mathbf{p}} + \mathbf{\Phi}_q\Delta\dot{\mathbf{q}} = \mathbf{0}, \\ &(R_{ij})_p\Delta\dot{\mathbf{p}} + (R_{ij})_q\Delta\dot{\mathbf{q}} = -(1+r_e)[(R_{ij})_p\dot{\mathbf{p}}(t_i^-) + (R_{ij})_q\dot{\mathbf{q}}(t_i^-)]. \end{aligned} \tag{8}$$

Eliminating $\mathbf{H}^{\lambda}$ and $\Delta\dot{\mathbf{p}}$ yields

$$\hat{\mathbf{P}}\Delta\dot{\mathbf{q}} = -(1+r_e)\hat{\mathbf{Z}}, \qquad \Delta\hat{\mathbf{M}}\Delta\dot{\mathbf{q}} = \Delta\hat{\mathbf{Q}}, \tag{9,10}$$

where $\hat{\mathbf{P}}$, $\hat{\mathbf{Z}}$, $\Delta\hat{\mathbf{M}}$, and $\Delta\hat{\mathbf{Q}}$ can be seen in reference [21].

The computational algorithm for dynamic simulation is described as follows:

(1) In the interval without impact, we integrate governing equation (5) of the slider–crank mechanism system from $\tau = 0$ to τ_i^-.
(2) From equations (9) and (10), we solve for the jump discontinuity of velocity $\Delta\dot{\mathbf{q}}$; then, the velocity after impact is obtained as

$$\dot{\mathbf{q}}(\tau_i^+) = \dot{\mathbf{q}}(\tau_i^-) + \Delta\dot{\mathbf{q}}. \tag{11}$$

(3) Finally, we compute the numerical integration of equation (5) with the new initial velocity $\dot{\mathbf{q}}(\tau_i^+)$ from $\tau = \tau_i^+$. However, the initial position remains the same, i.e., $\mathbf{q}(\tau_i^+) = \mathbf{q}(\tau_i^-)$.

3.2. THE CFM APPROACH

In general, the impact process may be considered in two phases: the compression phase and the restitution phase. The former starts at the relative normal velocity that is reduced to zero and lasts until the instantaneous common velocity of maximum compression. The latter starts at the maximum approach of the instantaneous common velocity and ends at the separation of two colliding bodies. The CFM approach [9] employs a logical spring–damper element to estimate the impact force between the two bodies i and j of a mechanism system as

$$F_{ij} = K\xi_{ij} + D\dot{\xi}_{ij}, \tag{12}$$

where K is the elastic spring coefficient, ξ_{ij} is the relative displacement or penetration between the surfaces of two colliding bodies, $\dot{\xi}_{ij}$ is the relative velocity, and D is the damping coefficient that can be represented as $\mu\dot{\xi}$, in which μ is called the hysteresis damping factor.

Following the process of reference [9], we can determine the coefficients K and D (or μ) of the CFM approach as

$$K = \frac{m^i m^j}{m^i + m^j}\left(\frac{\dot{\bar{\xi}}_{ij}}{\hat{\xi}_{ij}}\right)^2, \qquad \mu = \frac{3}{4}\frac{K(1-\alpha^2)\dot{\bar{\xi}}_{ij}^2}{(1/\bar{\beta})[\dot{\bar{\xi}}_{ij}^2 + \bar{\beta}^2\hat{\xi}_{ij}^2]^{3/2} - [\dot{\bar{\xi}}_{ij}^3/\bar{\beta}]}, \tag{13,14}$$

where $\dot{\bar{\xi}}_{ij}$ is the value of the initial relative penetration velocity, $\hat{\xi}_{ij}$ is the value of the maximum penetration, α is the coefficient of restitution between two colliding bodies, and $\bar{\beta} = K(m^i + m^j)/m^i m^j$.

Thus, the CFM described by equation (12) can be calculated by using equations (13) and (14). Then, during $\tau_i^- \leqslant \tau \leqslant \tau$ the DAE (3) can be rewritten in the matrix form as

$$\begin{bmatrix} \mathbf{M} & \mathbf{\Phi}_Q^{\mathrm{T}} \\ \mathbf{\Phi}_Q & \mathbf{0} \end{bmatrix}\begin{bmatrix} \ddot{\mathbf{Q}} \\ \boldsymbol{\lambda} \end{bmatrix} = \begin{bmatrix} \mathbf{Q}^{\mathrm{A}} - \mathbf{N}(\mathbf{Q}, \dot{\mathbf{Q}}) + \mathbf{Q}_F \\ \boldsymbol{\gamma} \end{bmatrix}, \tag{15}$$

where $\mathbf{Q}_F = \{\partial \xi_{ij}/\partial \mathbf{Q}\} F_{ij}$, in which F_{ij} is the impulse force between the two colliding bodies i and j. According to the decomposition of $\mathbf{Q}$ into $\mathbf{p}$ and $\mathbf{q}$, equation (15) becomes

$$\mathbf{M}^{pp}\ddot{\mathbf{p}} + \mathbf{M}^{pq}\ddot{\mathbf{q}} + \mathbf{\Phi}_p^{\mathrm{T}}\lambda = \mathbf{B}^p\mathbf{U} - \mathbf{N}^p + \mathbf{Q}_F^p,$$

$$\mathbf{M}^{qp}\ddot{\mathbf{p}} + \mathbf{M}^{qq}\ddot{\mathbf{q}} + \mathbf{\Phi}_q^{\mathrm{T}}\lambda = \mathbf{B}^q\mathbf{U} - \mathbf{N}^q + \mathbf{Q}_F^q,$$

$$\mathbf{\Phi}_p\ddot{\mathbf{p}} + \mathbf{\Phi}_q\ddot{\mathbf{q}} = \gamma. \tag{16}$$

Eliminating λ and $\ddot{\mathbf{p}}$ yields

$$\hat{\mathbf{M}}(\mathbf{q})\ddot{\mathbf{q}} + \hat{\mathbf{N}}(\mathbf{q}, \dot{\mathbf{q}}) = \hat{\mathbf{Q}}\mathbf{U} + \hat{\mathbf{Q}}_F, \tag{17}$$

where $\hat{\mathbf{M}}$, $\hat{\mathbf{N}}$, $\hat{\mathbf{Q}}$, and $\hat{\mathbf{Q}}_F$ can be seen in reference [21]. Equation (17) is a set of differential equations in terms of the independent co-ordinate $\mathbf{q}$ only and is an initial-value problem. The procedure of computational algorithm by using the CFM is similar to that of the GMB approach except that we solve equation (17) for the slider–crank mechanism system during the impact interval $\tau_i^- \leqslant \tau \leqslant \tau_i^+$.

3.3. THE CFM ASSOCIATED WITH THE EMC

The purpose of the CFM associated with the EMC is to evaluate two colliding bodies that are kinematically constrained to other bodies in the mechanism system. For instance, if the impact occurs not only on two colliding bodies i and j but also on two subsystems containing bodies i and j, respectively, then, the compensation of effective mass of subsystem must be considered. From the kinetic energy approach, the effective mass of other bodies in the subsystem can be estimated in the normal direction of impact.

To this end, the kinetic energy is written for subsystem i as

$$\tfrac{1}{2}\dot{\mathbf{Q}}^{i\mathrm{T}}\Xi^{i\mathrm{T}}\mathbf{M}\Xi^i\dot{\mathbf{Q}}^i = \tfrac{1}{2}\dot{\mathbf{Q}}^{i\mathrm{T}}\left(\frac{\partial \xi_{ij}}{\partial \mathbf{Q}}\right)^{i\mathrm{T}} m_f^i \left(\frac{\partial \xi_{ij}}{\partial \mathbf{Q}}\right)^i \dot{\mathbf{Q}}^i, \tag{18}$$

where Ξ^i is the diagonal matrix and m_f^i is the effective mass for body i. From equation (18), one obtains

$$m_f^i = \frac{\tfrac{1}{2}\dot{\mathbf{Q}}^{i\mathrm{T}}\Xi^{i\mathrm{T}}\mathbf{M}\Xi^i\dot{\mathbf{Q}}^i}{\tfrac{1}{2}\dot{\mathbf{Q}}^{i\mathrm{T}}(\partial \xi_{ij}/\partial \mathbf{Q})^{i\mathrm{T}}(\partial \xi_{ij}/\partial \mathbf{Q})^i\dot{\mathbf{Q}}^i}. \tag{19}$$

Following similar steps, one can obtain the effective mass m_f^j for body j.

The procedure of computational algorithm is as follows. Substituting the effective mass (19) into equation (13), one obtains the coefficient of spring. Using the damping coefficient (14), one obtains CFM (12) accounting for the effective mass in the mechanism system under impact.

4. DESIGN OF VARIABLE STRUCTURE CONTROLLER

In this section, the VSC algorithm is designed for tracking the crank angle and speed of system (6). The first objective is to track the crank angle of the slider–crank mechanism

associated with a flexible connecting rod. In most of the dynamic analyses of mechanism [6, 7], it was observed that as the desired crank angle is achieved the flexible vibrations are excited. In order to damp out the flexible vibrations, a stabilization controller by using pole placement technique is designed.

4.1. ANGULAR POSITION TRACKING CONTROLLER DESIGN

The flexible slider–crank mechanism is a single-input–single-output (SISO) system. A detailed derivation including the rigid-body motion and flexible vibration is presented in reference [7]. Rewriting equation (5), one obtains a second order non-linear coupled system of the general control form

$$\ddot{\mathbf{q}} = \mathbf{f}(\mathbf{q}, \dot{\mathbf{q}}) + \mathbf{G}(\mathbf{q}, \dot{\mathbf{q}})\mathbf{U}, \tag{20}$$

where

$$\mathbf{f}(\mathbf{q}, \dot{\mathbf{q}}) = -\hat{\mathbf{M}}^{-1}\hat{\mathbf{N}}, \qquad \mathbf{G}(\mathbf{q}, \dot{\mathbf{q}}) = \hat{\mathbf{M}}^{-1}\hat{\mathbf{Q}}.$$

The generalized co-ordinates $\mathbf{q} = [\theta\ \mathbf{g}]^{\mathrm{T}}$ include the crank angle θ and the vector of flexible modes $\mathbf{g} = [g_1\ g_2 \cdots g_m]$, and $\mathbf{U}$ is the control input current $[I_q^*]$ for the PM synchronous servo motor.

If the impact occurs, equation (17) can be rewritten as

$$\ddot{\mathbf{q}} = \mathbf{f}(\mathbf{q}, \dot{\mathbf{q}}) + \mathbf{G}(\mathbf{q}, \dot{\mathbf{q}})\mathbf{U} + \mathbf{Q}_a, \tag{21}$$

where $\mathbf{Q}_a = \hat{\mathbf{M}}^{-1}\hat{\mathbf{Q}}_F$ represents the generalized impulse force due to impact.

The control objective is to design a VSC law such that the crank angle θ can track the desired reference model trajectory θ_{rm}. The tracking error is defined as

$$e = \theta - \theta_{rm}. \tag{22}$$

Then, the error dynamics of the motor-controller flexible slider–crank mechanism system can be described as follows:

$$\begin{aligned} \dot{e} &= \dot{\theta} - \dot{\theta}_{rm}, \\ \ddot{e} &= \ddot{\theta} - \ddot{\theta}_{rm} \\ &= -\mathbf{A}_1\hat{\mathbf{N}} + \mathbf{A}_1\hat{\mathbf{Q}}\mathbf{U} - \ddot{\theta}_{rm}, \end{aligned} \tag{23}$$

where $\mathbf{A}_1$ is obtained from $\hat{\mathbf{M}}^{-1} = [\mathbf{A}_1\ \mathbf{A}_2]^{\mathrm{T}}$.

From the VSC methodology, we define a sliding surface $s = 0$ in the state space $\mathbf{R}^2$ by the switching function

$$s = \dot{e} + 2\varsigma\omega_n e + \omega_n^2 z_s, \tag{24}$$

where $z_s = \int_0^{\tau} e(\gamma)\,\mathrm{d}\gamma$. It is known [15] that once the state trajectory reaches the sliding surface $s = 0$, we have $e \to 0$ and also $\theta \to \theta_{rm}$ exponentially.

Now, it is assumed that the parameters of the flexible mechanism system are well known as the nominal condition. Differentiating switching function s and according to the error

dynamics of equation (23), the VSC control input $\mathbf{U}_{VSC}$ is found as

$$\mathbf{U}_{VSC} = -(\mathbf{A}_1\hat{\mathbf{Q}})^{-1}[W + k\,\mathrm{sgn}(s)], \tag{25}$$

where

$$W = 2\varsigma\omega_n\dot{e} + \omega_n^2 e - \ddot{\theta}_{rm} - \mathbf{A}_1\hat{\mathbf{N}},$$

K is the positive constant coefficient and the sign function is

$$\mathrm{sgn}(s) = \begin{cases} 1 & \text{if } s > 0, \\ -1 & \text{if } s < 0. \end{cases}$$

It should be noted that the sliding mode would occur along the sliding surface $s = 0$ only if the existence condition [21] $s\dot{s} < 0$ holds.

Theorem. *The tracking controller obtained by equation* (25) *makes the state trajectory of* s *confine to the sliding surface* $s = 0$; *therefore,* $e \to 0$ *and also* $\theta \to \theta_{rm}$ *as* $t \to \infty$.

Proof. According to the above theorem, applying the control input $\mathbf{U} = \mathbf{U}_{VSC}$, we have

$$\begin{aligned} s\dot{s} &= s(W + \mathbf{A}_1\hat{\mathbf{Q}}\mathbf{U}) \\ &= s\{W + \mathbf{A}_1\hat{\mathbf{Q}}\{-(\mathbf{A}_1\hat{\mathbf{Q}})^{-1}[W + k\,\mathrm{sgn}(s)]\}\} \\ &\leqslant -K|s| \\ &\leqslant 0. \end{aligned} \tag{26}$$

To alleviate the chattering phenomenon along the sliding surface $s = 0$, we adopt the quasi-linear mode controller [10], which replaces the discontinuous term of sign function of equation (25) by a continuous function inside a boundary layer around the sliding surface. Therefore, sgn(s) in equation (25) is replaced by the saturation function

$$sat\left(\frac{s}{\varepsilon}\right) = \begin{cases} 1 & \text{if } s > \varepsilon, \\ \dfrac{s}{\varepsilon} & \text{if } -\varepsilon \leqslant s \leqslant \varepsilon, \\ -1 & \text{if } s < -\varepsilon, \end{cases} \tag{27}$$

where $\varepsilon > 0$ is the width of the boundary layer. This limits the tracking error and guarantees an accuracy of ε order while alleviating the chattering phenomenon.

4.2. STABILIZER DESIGN

By using the tracking controller of equation (25), one can track a desired reference trajectory of crank angle. However, flexible vibrations of the slider–crank mechanism are excited during tracking control. Therefore, it is necessary to design a stabilizer to damp out the flexible vibrations.

4.2.1. *Linearization*

Let the stabilizer control input function $\mathbf{U}_s$ be

$$\mathbf{U}_s = S_d(\mathbf{A}_1\hat{\mathbf{Q}})^{-1}, \tag{28}$$

where S_d stands for the stabilizer control input gain, and will be obtained by pole placement technique in the next section. Substituting $\mathbf{U} = \mathbf{U}_{VSC} + \mathbf{U}_S$ into time derivative of s, one obtains

$$\dot{s} = -k\,sat(s) + S_d. \tag{29}$$

It is assumed that as the crank angle reaches a desired terminal value $\theta_{rm} = \theta^*$, i.e., $\theta \to \theta^*$, we have $\dot{\theta} \to 0$ and $\ddot{\theta} \to 0$ as $t \to \infty$. When the crank angle enters a small neighborhood of the desired one, that is $\theta \to \theta^*$, $\dot{\theta} \to 0$ and $\ddot{\theta} \to 0$, the motor-controller flexible slider–crank mechanism system can be well approximated by a linear system. Then, the stabilizer design based on the asymptotically linearized model is suitable [15]. Linearizing equation (29), one obtains

$$\dot{s} = -k\frac{s}{\varepsilon} + S_d. \tag{30}$$

Then, the tracking error can be expressed as

$$\Delta e = \theta - \theta^*, \qquad \Delta\mathbf{g} = \mathbf{g} - \mathbf{g}^*, \tag{31, 32}$$

where θ^* and $\mathbf{g}^*$ stand for the equilibrium point of the desired crank angle and the desired vector of flexible deflection respectively. Using equations (30) and (31) and substituting the time derivative of Δe into equation (24), we have

$$\Delta\dot{e} = -2\varsigma\omega_n\Delta e + s - \omega_n^2 z_s, \tag{33}$$

$$\Delta\ddot{e} = \omega_n^2(4\varsigma^2 - 1)\Delta e + \left(-2\varsigma\omega_n - \frac{k}{\varepsilon}\right)s + 2\varsigma\omega_n^3 z_s + S_d. \tag{34}$$

By using equations (31) and (32), equation (5) can be expanded by Taylor series about the equilibrium point θ^* and $\mathbf{g}^*$ as

$$\begin{bmatrix} \hat{\mathbf{M}}_{11}^* & \hat{\mathbf{M}}_{12}^* \\ \hat{\mathbf{M}}_{21}^* & \hat{\mathbf{M}}_{22}^* \end{bmatrix}\begin{bmatrix} \Delta\ddot{e} \\ \Delta\ddot{\mathbf{g}} \end{bmatrix} + \begin{bmatrix} \hat{\mathbf{N}}_{11}^* & \hat{\mathbf{N}}_{12}^* \\ \hat{\mathbf{N}}_{21}^* & \hat{\mathbf{N}}_{22}^* \end{bmatrix}\begin{bmatrix} \Delta e \\ \Delta\mathbf{g} \end{bmatrix} = \begin{bmatrix} \hat{\mathbf{Q}}_1^* \\ \hat{\mathbf{Q}}_2^* \end{bmatrix}\Delta\mathbf{U}, \tag{35}$$

where $\Delta\mathbf{U} = \mathbf{U} - \mathbf{U}^*$ and $\mathbf{U}^*$ is the control input current for the PM synchronous servo motor holding the crank angle at θ^*. From equation (35), one can describe the flexible dynamics as

$$\hat{\mathbf{M}}_{21}^*\Delta\ddot{e} + \hat{\mathbf{M}}_{22}^*\Delta\ddot{\mathbf{g}} + \hat{\mathbf{N}}_{21}^*\Delta e + \hat{\mathbf{N}}_{22}^*\Delta\mathbf{g} = \mathbf{0}. \tag{36}$$

Rewriting equation (36) yields

$$\Delta\ddot{\mathbf{g}} = -\hat{\mathbf{M}}_{22}^{*\,-1}(\hat{\mathbf{M}}_{21}^{*}\Delta\ddot{e} + \hat{\mathbf{N}}_{21}^{*}\Delta e + \hat{\mathbf{N}}_{22}^{*}\Delta\mathbf{g}). \tag{37}$$

Define the new state variable $\bar{\mathbf{X}} = (\Delta e\ s\ \Delta\mathbf{g}\ \Delta\dot{\mathbf{g}}\ z_s)^{\mathrm{T}} \in R^{2n+3}$. Substituting equation (34) into equation (37) and using equations (30) and (33), one obtains the complete linearized model as

$$\dot{\bar{\mathbf{X}}} = \bar{\mathbf{M}}\bar{\mathbf{X}} + S_d\bar{\mathbf{Q}}, \tag{38}$$

where $\bar{\mathbf{M}}$ and $\bar{\mathbf{Q}}$ can be seen in reference [21].

In order to obtain boundedness of the flexible modes, one must design a stabilizer controller $\mathbf{U}_s$ such that the zero dynamics of the system are stable. The zero dynamics are defined to be the residual motion of the flexible mechanism system when $s = 0$ and $\theta = \theta_{rm} = \theta^*$. This implies that θ and its time derivatives are identically zero. Obviously, when the crank angle is held constant, the zero dynamics essentially are flexible dynamics of the flexible slider–crank mechanism system. By setting the state variables $\Delta e = 0$, $s = 0$, and $z_s = 0$ in equation (38), one can obtain the zero dynamics as

$$\begin{bmatrix} \Delta\dot{\mathbf{g}} \\ \Delta\ddot{\mathbf{g}} \end{bmatrix} = \begin{bmatrix} \mathbf{0} & \mathbf{1} \\ \bar{\mathbf{M}}_{43} & \mathbf{0} \end{bmatrix} \begin{bmatrix} \Delta\mathbf{g} \\ \Delta\dot{\mathbf{g}} \end{bmatrix}. \tag{39}$$

The characteristic equation of the zero dynamics (39) yields

$$\begin{aligned} D(\lambda) &= \det(\lambda^2 I - \bar{\mathbf{M}}_{43}) \\ &= \det[\lambda^2 - (-\hat{\mathbf{M}}_{22}^{*\,-1}\hat{\mathbf{N}}_{22}^{*})] \\ &= \det(\hat{\mathbf{M}}_{22}^{*}\lambda^2 + \hat{\mathbf{N}}_{22}^{*}) \\ &= 0. \end{aligned} \tag{40}$$

It is easy to find that the roots of the characteristic equation associated with the flexible modes are purely imaginary. Thus, when the system reaches the desired crank angle via the VSC controller, it is obvious that the flexible modes have oscillatory responses.

4.2.2. *Pole placement technique*

Since the linearized model of equation (38) is not stable due to the flexible dynamics, a linear stabilizer is designed via the pole placement technique to move the flexible dynamics poles on the imaginary axis to the left-hand side of the s-plane such that the complete linearized model of equation (38) is stable. The stabilizer control input gain S_d is designed as

$$S_d = -\mathbf{L}\bar{\mathbf{X}}, \tag{41}$$

where $\mathbf{L}$ stands for the stabilizer feedback gain matrix which regulates the existing imaginary poles of the linearized model (38) to the left-hand side of the s-plane. Then, the linearized model of equation (38) for stabilization can be written as

$$\dot{\bar{\mathbf{X}}} = (\bar{\mathbf{M}} - \bar{\mathbf{Q}}\mathbf{L})\bar{\mathbf{X}}. \tag{42}$$

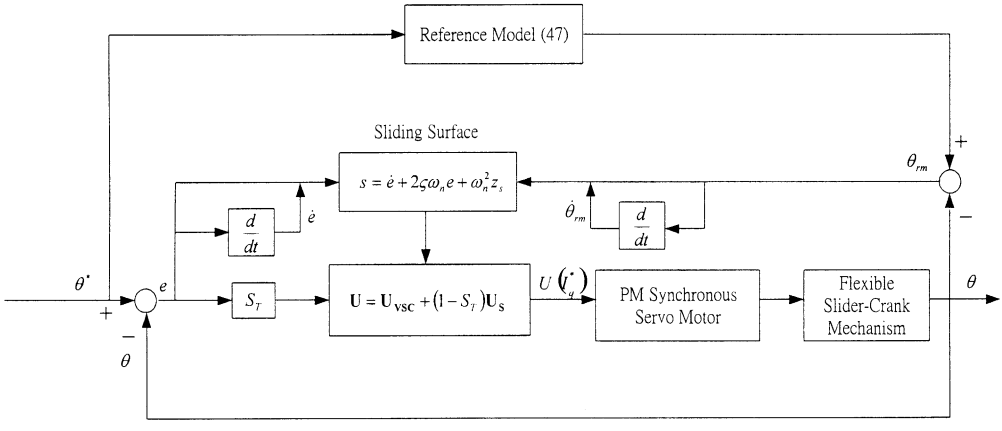

Figure 2. The block diagram of the motor-controller flexible slider–crank mechanism by using the VSC controller and the stabilizer design.

The total controller is finally defined as

$$\mathbf{U} = \mathbf{U}_{VSC} + (1 - S_T)\mathbf{U}_s, \tag{43}$$

where

$$S_T = \begin{cases} 1 & \text{if } \tau < \tau_t, \\ 0 & \text{if } \tau \geqslant \tau_t \end{cases}$$

and τ_t is the switching time.

4.3. COMPUTATIONAL ALGORITHM

The procedure of computational algorithm for the dynamic simulation is described as follows:

(1) First, one tracks the crank angle to the desired one for the time interval $0 < \tau < \tau_t$ by using the controller $\mathbf{U} = \mathbf{U}_{VSC}$ that is based on the VSC methodology.
(2) Although the crank angle enters a small neighborhood of the desired one, i.e., $\theta \to \theta^*$, $\dot{\theta} \to 0$ and $\ddot{\theta} \to 0$, the flexible vibrations are excited. Thus, the VSC input must be combined with a linear stabilizer of equations (28) and (41) to damp out the flexible vibrations. Thus, the controller is $\mathbf{U} = \mathbf{U}_{VSC} + \mathbf{U}_S$ for $\tau \geqslant \tau_t$.
(3) The block diagram of the VSC controller and the stabilizer design is shown in Figure 2.

5. NUMERICAL RESULTS

In the following numerical simulations, the parameters of the PM synchronous servo motor system are taken from reference [22]. The parameters of the flexible slider–crank mechanism are chosen as the same as those of reference [7] and the conditions under impact are considered as those of reference [9]. The input gains of the control law are

selected as

$$\varsigma = 0{\cdot}707, \qquad \omega_n = 3, \qquad k = 3, \qquad \varepsilon = 0{\cdot}5.$$

In the dynamic analysis, the DAE of the motor-controller flexible slider–crank mechanism system may be reordered and partitioned by the decomposition of $\mathbf{Q} = [\phi\ \theta\ \mathbf{g}]^{\mathrm{T}} = [\mathbf{p}^{\mathrm{T}}\,\mathbf{q}^{\mathrm{T}}]^{\mathrm{T}}$. The elements of vectors $\mathbf{p}$, $\mathbf{q}$ and matrices $\mathbf{\Phi}_p$, $\mathbf{\Phi}_q$, $\mathbf{M}^{pp}$, $\mathbf{M}^{pq}$, $\mathbf{M}^{qp}$, $\mathbf{M}^{qq}$, $\mathbf{N}^p$, $\mathbf{N}^q$, $\mathbf{B}^p$, $\mathbf{B}^q$, $(R_{ij})_p$, $(R_{ij})_q$, $\mathbf{Q}_F^p$ and $\mathbf{Q}_F^q$ for the flexible slider–crank mechanism are detailed in reference [21].

5.1. SPEED TRACKING CONTROL

5.1.1. *Constant angular speed*

First, the crank rotates with a constant angular speed $\dot{\theta}(\tau) = 1$. The initial conditions are $\mathbf{q}(0) = \mathbf{0}$, and $\dot{\mathbf{q}}(0) = [1\ \mathbf{0}]^{\mathrm{T}}$. The results in Figure 3 show the motion-induced vibrations of the first mode g_1 (solid line), and the second mode g_2 (dash line) of the flexible connecting rod. It is seen that the responses of the second mode are only small percentages of those of the first mode. It is also seen from Figure 3 that the transverse amplitudes are non-linear.

5.1.2. *Constant angular speed control*

The speed controller design is performed in this section. The tracking error is defined as

$$e = \int_0^{\tau} (\dot{\theta} - \omega_{rm})\,\mathrm{d}t, \tag{44}$$

where $\omega_{rm}(t)$ stands for the desired reference model trajectory of the crank angular speed. The error dynamics of the motor-controller flexible slider–crank mechanism system is the same as equation (23). Similarly, the VSC control input of the speed tracking controller can be found as

$$\mathbf{U}_{VSC} = -(\mathbf{A}_1\hat{\mathbf{Q}})^{-1}[W + k\,\mathrm{sgn}(s)], \tag{45}$$

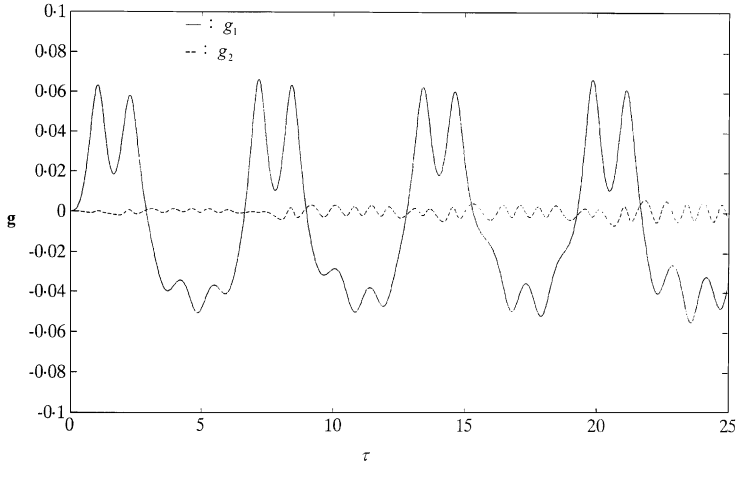

Figure 3. Motion-induced vibrations of the first (——) and second (– – –) modes of transverse amplitudes of the flexible connecting rod with a constant crank angular speed $\dot{\theta}(\tau) = 1$.

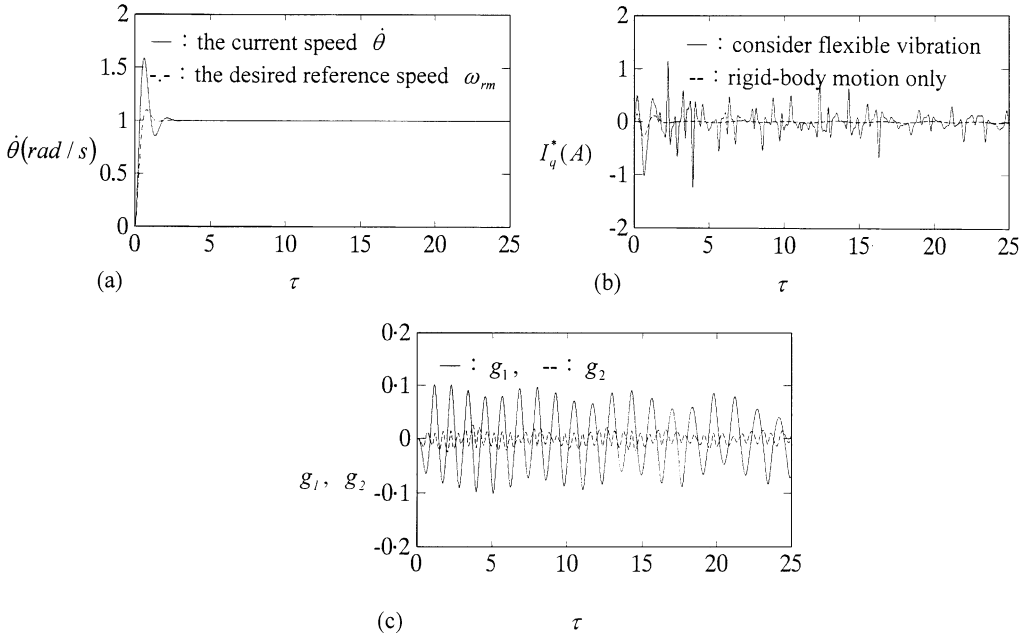

Figure 4. Comparison results of speed tracking controller associated with and without considering the flexible vibration: (a) the crank angular speed, (b) the control input I_q^*, and (c) the first two modes of transverse amplitudes.

where

$$W = 2\varsigma\omega_n\dot{e} + \omega_n^2 e - \dot{\omega}_{rm} - \mathbf{A}_1\hat{\mathbf{N}}.$$

In order to avoid a control input current with jumps, a second order reference model [15] for speed tracking trajectory is chosen as

$$\ddot{\omega}_{rm} + (2\varsigma_r\omega_{nr} + \lambda_r)\dot{\omega}_{rm} + 2(\varsigma_r\omega_{nr}\lambda_r + \omega_{nr}^2)\omega_{rm} = 2(\varsigma_r\omega_{nr}\lambda_r + \omega_{nr}^2)\dot{\theta}^*, \tag{46}$$

where $\varsigma_r = 0{\cdot}707$, $\omega_{nr} = 2{\cdot}828$, $\lambda_r = 2$, $\omega_{rm}(0) = \dot{\omega}_{rm}(0) = 0$, and $\dot{\theta}^*(\tau) = 1$. Here, the reference model is used to specify the ideal speed response of the motor-controller flexible slider–crank mechanism system.

Figure 4(a–c) compares the results of speed tracking controller (45) associated with and without considering the flexible vibrations. The initial conditions are all zero. In Figure 4(a), the crank transient speed (solid line) is the same for the system with and without considering the flexible vibrations, and is larger than the desired reference speed (dash–dotted line). The speeds are almost the same after $\tau = 3$. In Figure 4(b), the control input I_q^* has a larger value than that without considering the flexible vibrations. This is because the flexible vibrations affect reversely the rigid-body motion, and then the control input current. The excited transverse amplitudes of the first two modes shown in Figure 4(c) are larger than those with $\theta(\tau) = 1$ shown in Figure 3. It is seen from Figure 4(a–c) that the speed controller (45) effectively controls the speed to the desired one, but the flexible vibrations are also excited.

5.2. ANGULAR POSITION TRACKING

The poles of $\bar{\mathbf{M}}$ of equation (38) can be found as -6, $-2{\cdot}121 \pm \mathrm{j}2{\cdot}121$, $\pm\mathrm{j}$, $\pm\mathrm{j}4$. It is known from equation (40) that the purely imaginary pairs occur due to the flexible modes.

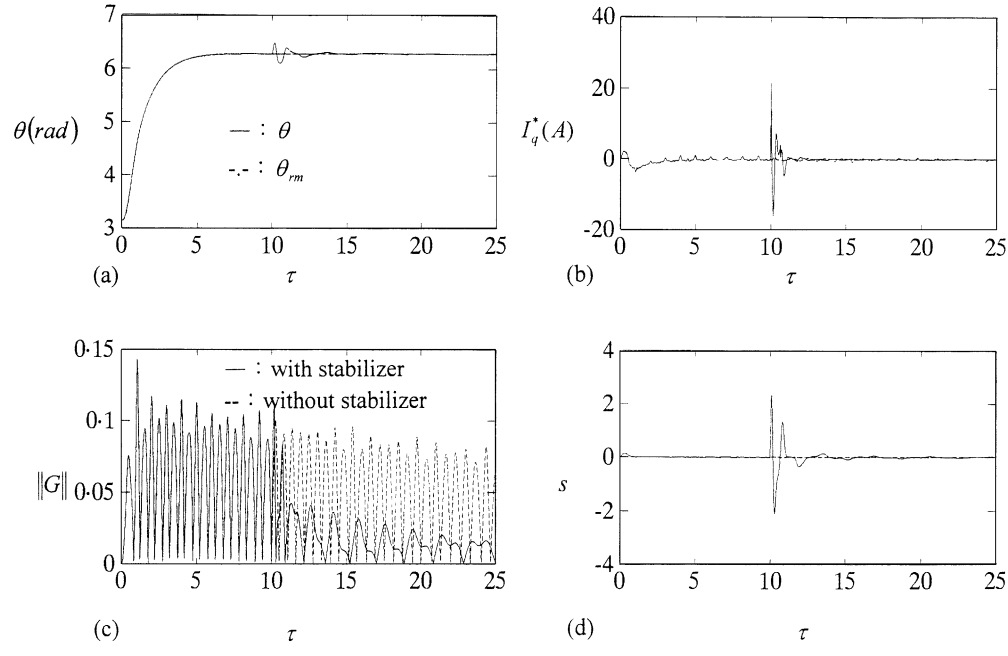

Figure 5. Comparison results of the VSC controller with and without the stabilizer design: (a) the crank angle, (b) the control input I_q^*, (c) the amplitude norm $\|G\|$, and (d) the sliding surface s.

The pole placement technique is used to move the poles of $\bar{\mathbf{M}}$ to the left-hand side of the s-plane as -6, $-2{\cdot}121 \pm j2{\cdot}121$, $-1 \pm j$, $-1 \pm j4$. Then, the stabilizer feedback gains matrix $\mathbf{L}$ is obtained by solving equation (42) as

$$\mathbf{L} = [-3{\cdot}3926 \;\; 16{\cdot}9836 \;\; -47{\cdot}1764 \;\; -159{\cdot}2069 \;\; 63{\cdot}2559 \;\; 9{\cdot}4521 \;\; -2{\cdot}5594].$$

A third order reference model of the form [15]

$$\dddot{\theta}_{rm} + (2\varsigma_r\omega_{nr} + \lambda_r)\ddot{\theta}_{rm} + 2(\varsigma_r\omega_{nr}\lambda_r + \omega_{nr}^2)\dot{\theta}_{rm} + \omega_{nr}^2\lambda_r\theta_{rm} = \omega_{nr}^2\lambda_r\theta^* \tag{47}$$

with $\varsigma_r = 0{\cdot}707$, $\omega_{nr} = 2{\cdot}828$, $\lambda_r = 2$, $\theta_{rm}(0) = \pi$, $\dot{\theta}_{rm}(0) = 0$, and $\theta^* = 2\pi$ is chosen for the angular position tracking. In the simulations, the control objective is to track the crank angular position from $\theta(0) = \pi$ to $\theta^* = 2\pi$. For the flexible vibrations, it is convenient to introduce the norm of the generalized co-ordinates, $\|G\| = \sqrt{g_1^2 + g_2^2 + \cdots + g_m^2}$, where m is the maximum mode number, and $m = 2$ in this paper.

Numerical results are shown in Figure 5(a–d) and are compared with and without the stabilizer control algorithm. The stabilizer control input function $\mathbf{U}_S$ starts at $\tau_1 = 10$ when the crank angle has entered a small neighborhood of the desired crank angle. Meanwhile, it can be seen from Figure 5(a, b, d) that a transient jump occurs because the control law changes from $\mathbf{U}_{VSC}$ to $\mathbf{U}_{VSC} + \mathbf{U}_S$ for damping the flexible vibrations. Figure 5(a) shows the controlled crank angle and the desired one (47). They are almost the same from $\tau = 0$ to 10. Figure 5(b) shows the jump of the control input current when the stabilizer starts, and gradually vanishes in a finite time. The flexible vibrations are excited in Figure 5(c) under tracking the desired angular model reference trajectory (47) via the VSC controller. In order to damp out the flexible vibrations, the stabilizer is exerted in the controller design. It is

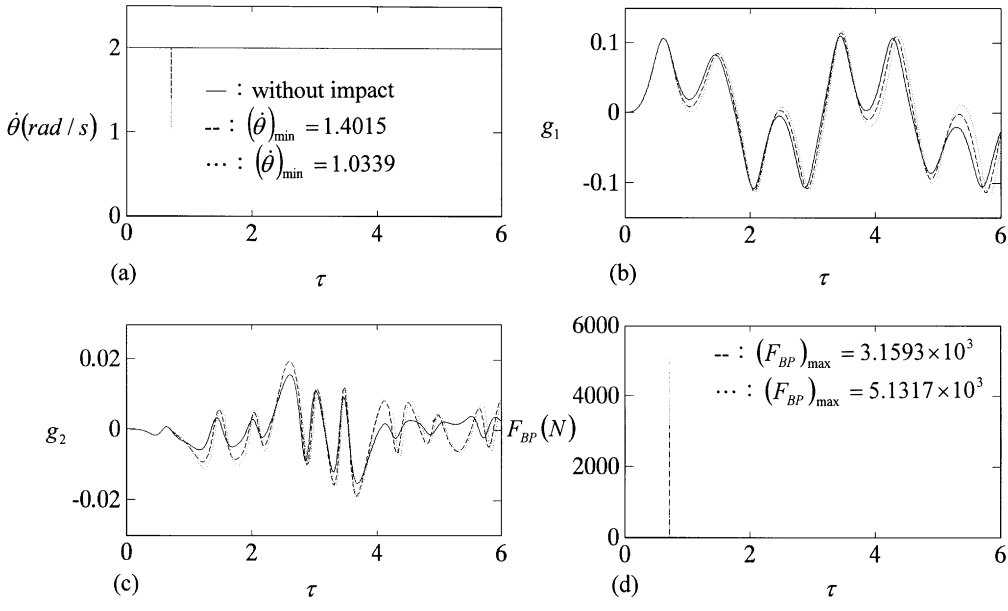

Figure 6. Comparison results of the motion-induced vibrations of the flexible connecting rod with and without undergoing impact: (a) the constant crank angular speed, (b) the first mode of transverse amplitude g_1, (c) the second mode of transverse amplitude g_2, and (d) the impact forces between sliders B and P. ——: without impact, – – –: the CFM approach, ···: the CFM associated with the EMC.

observed from Figure 5(c) that the amplitude norm of flexible vibrations is suppressed by combining the VSC controller and the stabilizer design. In Figure 5(d), the sliding surface starts as $s = 0$ because there is no initial tracking error. The sliding surface also has a jump when the stabilizer starts, and gradually vanishes in a finite time.

5.3. SPEED TRACKING CONTROL WITH IMPACT

Figure 6(a–d) compares the results for the motion-induced vibrations of the flexible connecting rod with and without undergoing impact. The constant crank angular speed is $\dot{\theta}(\tau) = 2$. The impact is assumed to take place at half of the stroke of slider B, i.e., the position of the free slider P is located at $x_P = x_B + \frac{1}{2}(x_B^* - x_B)$. The block diagram of the VSC algorithm and the stabilizer design under impact is similar to Figure 2. Since the control objective is to track the crank angular position, the values of θ^* and θ should be transferred to x_B^* and x_B by using the relation

$$x_B = r\cos\theta + [l^2 - r^2\sin^2\theta]^{1/2}. \tag{48}$$

It is clear that the constant crank angular speed has a larger discontinuous jump under impact via the CFM associated with the EMC (dotted line) as shown in Figure 6(a). It is also obvious from Figure 6(b, c) that the motion-induced vibrations for the first two modes of transverse amplitudes are increased under impact. The impact forces between sliders B and P are compared in Figure 6(d). The CFM associated with the EMC has a larger impact force. The numerical results via the GMB approach cannot be calculated using Runge–Kutta method because there is no time interval for the impact to occur.

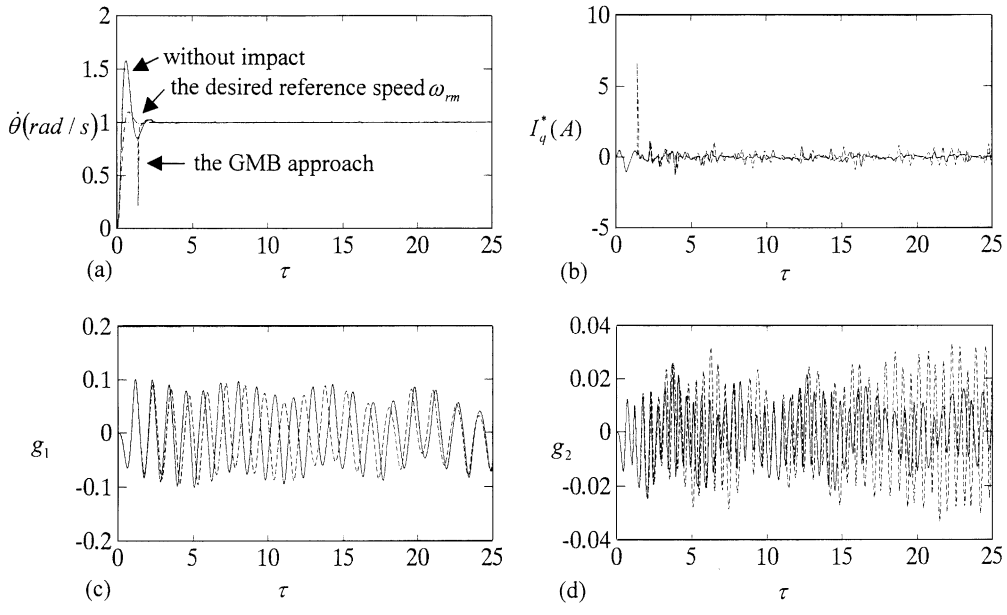

Figure 7. Comparison results of speed tracking controller by considering flexible vibrations and undergoing impact: (a) the crank angular speed $\dot{\theta}$, (b) the control input I_q^*, (c) the first mode of transverse amplitude g_1, and (d) the second mode of transverse amplitude g_2.

The simulation results for the speed tracking controller by considering flexible vibrations and undergoing impact via the GMB approach are compared in Figure 7(a–d). It is observed that the crank angular speed in Figure 7(a) and the control input I_q^* in Figure 7(b) have a discontinuous jump under impact. It is seen that the first-mode transverse amplitude g_1 has a phase lag due to the impact as shown in Figure 7(c), and the excited second-mode transverse amplitude g_2 is larger than that without impact as shown in Figure 7(d). The generalized impulse is found as 0·4155 N s for the GMB approach.

5.4. ANGULAR POSITION TRACKING WITH IMPACT

In the following simulations, the control objective is to track the crank angular position from $\theta(0) = \pi$ to $\theta^* = 2\pi$. The simulation results of nominal case under impact via the GMB approach are shown in Figure 8(a–c). It is obvious that the crank angular speed has a jump about $\tau = 1{\cdot}5$ for the flexible slider–crank mechanism undergoing impact as shown in Figure 8(a). The control input I_q^* overcoming the sudden impact also has a discontinuous jump as shown in Figure 8(b). From Figure 8(c), it is clear that the flexible vibrations have the phase lag due to a small impact. In order to track the desired angular model reference trajectory of the crank, the VSC controller is employed. Similarly, in order to eliminate the flexible vibrations of the connecting rod, the stabilizer is also exerted in the controller design under impact. It is observed that the transverse amplitude norm is suppressed as shown in Figure 8(c). It can be calculated from equation (10) that the generalized impulse is 0·5996 N s.

Furthermore, comparison results of the impact durations ($\Delta\tau = |\tau_i^+ - \tau_i^-|$) and impact forces for the CFM approach, and the CFM associated with the EMC between sliders B and P are summarized in Table 1. It is found that the CFM associated with the EMC has the largest value of impact duration and force.

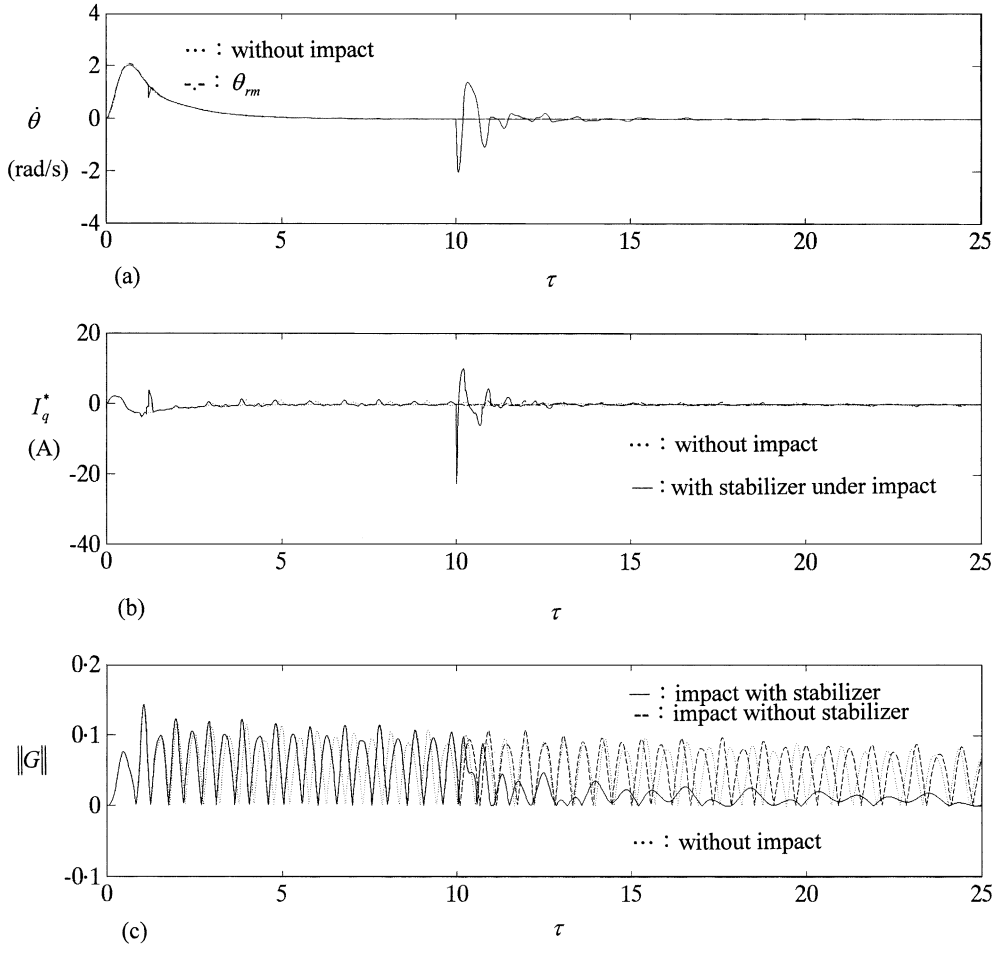

Figure 8. Comparison results of the VSC controller with and without the stabilizer design: (a) the crank angular speed $\dot{\theta}$, (b) the control input I_q^*, and (c) the amplitude norm $\|G\|$.

TABLE 1

Compare the impact durations and impact forces between sliders B and P of the motor-controller flexible slider–crank mechanism ($(F_{BP})_{max}$ unit: N)

Numerical results	Approaches of impact analysis	
	The CFM approach	The CFM associated with the EMC
Constant angular speed	$\Delta\tau = 3{\cdot}64 \times 10^{-3}$ $(F_{BP})_{max} = 3{\cdot}1593 \times 10^{3}$	$\Delta\tau = 4{\cdot}02 \times 10^{-3}$ $(F_{BP})_{max} = 5{\cdot}1317 \times 10^{3}$
Constant angular speed control	$\Delta\tau = 4{\cdot}27 \times 10^{-3}$ $(F_{BP})_{max} = 9{\cdot}6203 \times 10^{2}$	$\Delta\tau = 5{\cdot}15 \times 10^{-3}$ $(F_{BP})_{max} = 1{\cdot}6886 \times 10^{3}$
Angular position regulation	$\Delta\tau = 3{\cdot}14 \times 10^{-3}$ $(F_{BP})_{max} = 1{\cdot}8487 \times 10^{3}$	$\Delta\tau = 4{\cdot}02 \times 10^{-3}$ $(F_{BP})_{max} = 3{\cdot}2653 \times 10^{3}$

6. CONCLUSIONS

The flexible vibrations always occur during the motion control of a mechanism system. Angular position tracking of a motor-controller flexible slider–crank mechanism with and without impact by using the VSC controller and the stabilizer has successfully been performed. The stabilizer design is based on the pole placement technique to control the flexible vibrations of the slider–crank mechanism. The controller design is two-fold. First, the control strategy is to track the crank angle via the VSC controller. Second, as the crank angle trajectory enters the vicinity of the desired one, the stabilizer control input starts. From the simulation results, it is shown that the VSC controller involving a stabilizer design can both track the crank angular position and speed and suppress the flexible vibrations simultaneously. Moreover, the impact force and duration via the CFM associated with the EMC are larger than those of the CFM because of introducing the effective masses of the subsystem into the two colliding bodies.

ACKNOWLEDGMENTS

The authors are greatly indebted to the National Science Council of R.O.C. for the support of the research through contract No. NSC 89-2213-E-033-044.

REFERENCES

1. A. G. ERDMAN 1993 *Modern Kinematics, Developments in the Last Forty Years*. New York: Wiley & Sons, Inc.; chapter 9.
2. J. LIEH 1994 *Mechanism and Machine Theory* **29**, 139–147. Dynamic modeling of a slider–crank mechanism with coupler and joint flexibility.
3. B. FALLAHI, S. LAI and S. VENKAT 1995 *American Society of Mechanical Engineers Journal of Dynamic Systems, Measurement, and Control* **117**, 329–335. A finite element formulation of a flexible slider crank mechanism using local coordinates.
4. R. F. FUNG 1996 *American Society of Mechanical Engineers Journal of Vibration and Acoustics* **118**, 687–689. Dynamic analysis of the flexible connecting rod of a slider–crank mechanism.
5. K. M. HSIAO and R. T. YANG 1996 *Journal of Sound and Vibration* **190**, 177–194. Effect of member initial curvature on a flexible mechanism response.
6. R. F. FUNG and H. H. CHEN 1997 *Journal of Sound and Vibration* **199**, 237–251. Steady-state response of the flexible connecting rod of a slider–crank mechanism with time-dependent boundary condition.
7. R. F. FUNG and K. W. CHEN 1998 *Journal of Sound and Vibration* **214**, 605–637. Dynamic analysis and vibration control of a flexible slider–crank mechanism using PM synchronous servo motor drive.
8. Y. A. KHULIEF and A. A. SHABANA 1986 *American Society of Mechanical Engineers Journal of Mechanisms, Transactions, and Automation in Design* **108**, 38–45. Dynamic analysis of constrained system of rigid and flexible bodies with intermittent motion.
9. Y. A. KHULIEF and A. A. SHABANA 1987 *Mechanism and Machine Theory* **22**, 213–224. A continuous force model for the impact analysis of flexible multibody systems.
10. J. J. E. SLOTINE and W. P. LI 1991 *Applied Nonlinear Control*. Englewood Cliffs, NJ: Prentice-Hall.
11. V. I. UTKIN 1992 *Sliding Modes in Control and Optimization*. New York: Springer-Verlag.
12. K. S. YEUNG and Y. P. CHEN 1989 *International Journal of Control* **49**, 1965–1978. Regulation of a one-link flexible robot arm using sliding-mode technique.
13. K. S. YEUNG and Y. P. CHEN 1990 *International Journal of Control* **52**, 101–117. Sliding-mode controller design of a single-link flexible manipulator under gravity.
14. Y. P. CHEN and K. S. YEUNG 1991 *International Journal of Control* **54**, 257–278. Sliding-mode control of multi-link flexible manipulators.
15. P. J. NATHAN and S. N. SINGH 1991 *American Society of Mechanical Engineers Journal of Dynamic Systems, Measurement, and Control* **113**, 669–676. Sliding mode control and elastic mode stabilization of a robotic arm with flexible links.

16. A. FICOLA, M. L. CAVA and P. MURAVA 1992 *IFAC Motion Control for Intelligent Automation*, October, 27–29. A simplified strategy to implement sliding mode control of a two-joints robot with a flexible forearm.
17. S. B. CHOI, C. C. CHEONG and H. C. SHIN 1995 *Journal of Sound and Vibration* **179**, 737–748. Sliding mode control of vibration in a single-link flexible arm with parameter variations.
18. E. N. PARVIZ 1988 *Computer-Aided Analysis of Mechanical System*. Englewood Cliffs, NJ: Prentice-Hall.
19. E. J. HAUG 1992 *Intermediate Dynamics*. Englewood Cliffs, NJ: Prentice-Hall.
20. G. D. J. JAVIOR 1994 *Kinematic and Dynamic Simulation of Multibody Systems*: *the Real Time Challenge*. New York: Springer-Verlag; chapter 10.
21. J. W. WU 2000 *Master's Thesis*, *Chung Yuan Christian University*, *Taiwan*. Variable structure control of the motor-flexible mechanism system.
22. J. I. UTKIN 1993 *IEEE Transactions on Industrial Electronics* **40**, 23–36. Sliding mode control design principles and applications to electric drives.